Geophysical Research Letters

RESEARCH LETTER
10.1029/2024GL108395

Unraveling the Extensive Impact of Subthermocline Eddies on the Western Pacific Undercurrent System

Fuad Azminuddin[1], Chan Joo Jang[1,2], Raden Dwi Susanto[3], and Saat Mubarrok[1,2,4]

[1]Ocean Circulation and Climate Research Department, Korea Institute of Ocean Science and Technology, Busan, Republic of Korea, [2]Department of Ocean Science, University of Science and Technology, Daejeon, Republic of Korea, [3]Department of Atmospheric and Oceanic Science & Marine-Estuarine Environmental Sciences, University of Maryland, College Park, MD, USA, [4]Research Group of Oceanography, Bandung Institute of Technology, Bandung, Indonesia

Abstract Subthermocline eddies (SEs) influencing ocean circulation are progressively known, yet their extensive impact on the western Pacific undercurrent system remains largely unexplored and, in some regions, often underestimated. Okubo-Weiss parameter analysis reveals a distinctive meridional pattern of cyclonic and anticyclonic SE distribution in the interior western Pacific basin that aligns with zonally elongated mean flows. These westward-propagating SEs play a pivotal role in regulating the formation of zonal undercurrents, particularly off-equatorial regions, through the convergence of eddy potential vorticity flux. Along the Pacific western boundary region, anticyclonic SEs typically enhance (reverse) the velocity of boundary currents flowing northward (southward), primarily through barotropic energy conversion, while cyclonic SEs do the opposite. To summarize, we provide a schematic map of the circulation system in the western Pacific and emphasize the interconnected framework of undercurrents, particularly in relation to SEs.

Plain Language Summary Subthermocline eddies (SEs) are widespread in the western Pacific Ocean, varying in size, depth, and speed. We've learned quite a bit about SEs and their influence on ocean circulation. However, their significant impact on the undercurrent system in the western Pacific is still not well understood and, in some regions, often underestimated. Using an eddy identification method, we have uncovered a pattern of SEs in the western Pacific that matches the alternating eastward mean flows. These SEs appear to play a role in shaping the tropical-subtropical eastward undercurrent system. Along the western boundary, the northward (southward) undercurrents are strengthened by the SEs spinning clockwise (counterclockwise). In summary, we provide a map of the western Pacific circulation system and highlight the interconnected relationships between undercurrents and SEs.

Key Points:

- A meridional pattern of Subthermocline eddies (SEs) that aligns with the western Pacific zonal undercurrents has been revealed
- Off-equatorial eastward undercurrents arise from the convergence of cyclonic (anticyclonic) swirling motions from the north (south)
- Along the western boundary, SEs significantly modulate the boundary undercurrents

Supporting Information:

Supporting Information may be found in the online version of this article.

Correspondence to:

F. Azminuddin and C. J. Jang,
fuad.azminuddin@gmail.com;
cjjang@kiost.ac.kr

Citation:

Azminuddin, F., Jang, C. J., Susanto, R. D., & Mubarrok, S. (2024). Unraveling the extensive impact of subthermocline eddies on the western Pacific undercurrent system. *Geophysical Research Letters*, *51*, e2024GL108395. https://doi.org/10.1029/2024GL108395

Received 18 JAN 2024
Accepted 26 AUG 2024

1. Introduction

Oceanic eddies are swirling water motions with a lateral (temporal) scale of tens to hundreds of kilometers (days to months), known as mesoscale, and approximately follow a geostrophic (hydrostatic) balance in the horizontal (vertical) plane (Robinson, 1983). The majority of them exhibit strong nonlinearity ($U/c > 1$) (Chelton et al., 2011), where the average rotational speed (U) is faster than its translation speed (c). Consequently, they can trap fluid as they translate, playing a role in distributing oceanic heat, salt, biogeochemical tracers, and pollutants (Danabasoglu et al., 1994; Raeisi et al., 2020; Q. Wang et al., 2022). Oceanic eddies can also modulate the strength and direction of major ocean currents and gyres, alternating their paths and intensities (Beech et al., 2022; McWilliams, 2008).

Our understanding of surface eddies has significantly improved with the aid of satellite altimetry. However, information about those below the thermocline is very limited, mainly due to the paucity of available observational data, which is often obtained from sporadic in situ measurements. Subthermocline eddies (SEs), typically characterized by lens-like vertical structures (Song et al., 2022), are mostly invisible at the surface. Nevertheless, they can significantly affect the circulation and transport of various properties in the ocean (e.g., heat, salt, and oxygen) (McCoy et al., 2020; Nan et al., 2017; Thomsen et al., 2016; F. Wang et al., 2016).

The generation of SEs is typically triggered by the instability of undercurrents or planetary waves. Qiu et al. (2015) suggested that the formation of westward-propagating SEs in the northwestern Pacific is primarily driven by the nonlinear triad instability of wind-forced annual baroclinic Rossby waves. These eddies emerge when westward-propagating Rossby waves break down due to the nonlinear triad instability. Additionally,

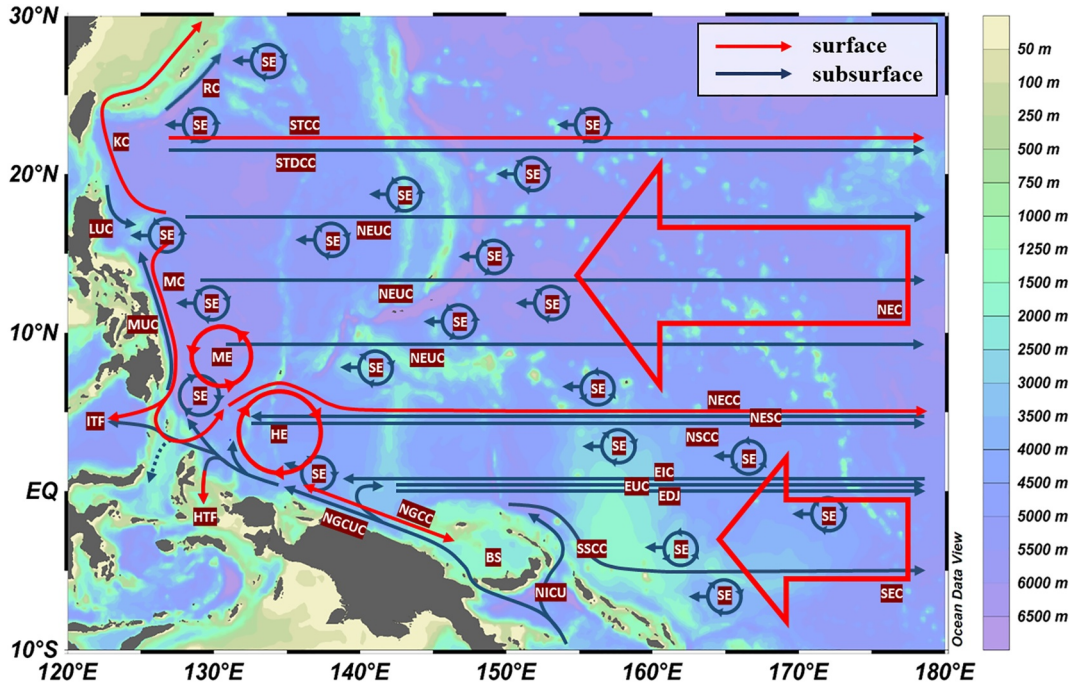

Figure 1. General pattern of the surface (red arrows) and subsurface (blue arrows) currents and eddies in the western Pacific. The surface currents and eddies are the North Equatorial Current, the Kuroshio Current, the Mindanao Current, the Subtropical Countercurrent, the North Equatorial Countercurrent, the South Equatorial Current, the New Guinea Coastal Current, the Indonesian Throughflow, Halmahera Throughflow, the Halmahera Eddy, and the Mindanao Eddy. The subsurface currents and eddies are the North Equatorial Undercurrent, the Subtropical Deep Countercurrent, the Ryukyu Current, the Luzon Undercurrent, the Mindanao Undercurrent, the North Equatorial Subsurface Current, the North Subsurface Countercurrent, the Equatorial Undercurrent, the South Subsurface Countercurrent, Equatorial Intermediate Current, Equatorial Deep Jets, the New Guinea Coastal Undercurrent, the New Ireland Coastal Undercurrent, and the Subthermocline Eddy. Figure adapted from Cravatte et al. (2012), Kashino et al. (2013), Qiu et al. (2013), Thoppil et al. (2016), Delpech et al. (2020), Hu et al. (2020), X. Li et al. (2020), Azminuddin et al. (2021), L. Zhang et al. (2021), and Azminuddin, Jang, and Jeon (2022).

Chiang et al. (2015) proposed that the generation of these SEs can be attributed to the meridional movements of the westward-flowing North Equatorial Current at the surface and the eastward-flowing North Equatorial Undercurrent (NEUC) below the thermocline, along with their interactions with the underlying topography.

Based on sporadic in situ observations and Argo float data, SEs have been observed in many parts of the global ocean, including four major ocean basins (Pacific, Atlantic, Indian, and Southern Oceans) and some marginal seas (e.g., Mediterranean Sea, East Sea, and South China Sea) (Richardson et al., 2000; Xu et al., 2019; Yang et al., 2019; Z. Zhang et al., 2017). Past studies have revealed the presence of mesoscale SEs in most western Pacific regions, exhibiting varying horizontal length scales (80–300 km), core depths (200–600 m), and translation speeds (6–13 cm s^{-1}) (Chiang & Qu, 2013; Chiang et al., 2015; Nan et al., 2017; Xu et al., 2019).

The western Pacific is characterized by a complex ocean circulation system, including narrow alternating zonal flows and intense boundary currents (see Figure 1). This regional current system plays a critical role in shaping the western Pacific warm pool, a large area of warm water with sea surface temperatures above 28°C, and influencing the life cycle of El Niño-Southern Oscillation, making it a crucial element for the global climate (Hu & Cui, 1991; Hu et al., 2020). SEs influencing the western Pacific circulation have been progressively known, but, in some regions, their impacts are often underestimated and sporadically assessed (Azminuddin et al., 2021; Chiang & Qu, 2013; Qiu et al., 2013; Yang et al., 2019; L. Zhang et al., 2014). This paper aims to elucidate the potential extensive impact of mesoscale SEs on the regional undercurrent system in the western Pacific (west of 180°E and 10°S to 30°N), encompassing both the interior basin and western boundary regions.

2. Methods

2.1. Eddy Identification Methods

This study utilizes the eddy kinetic energy (EKE) and Okubo-Weiss parameter (OWP) methods to identify SEs using the velocity field data from the Global Ocean Reanalysis and Simulation Version 4 (GLORYS2V4). GLORYS2V4 is a global ocean reanalysis data set, available at Mercator Ocean (https://marine.copernicus.eu). This model has a horizontal resolution of 0.25° × 0.25° and encompasses 75 vertical layers. The available daily data spans from 1993 to 2020. In our recent studies (Azminuddin et al., 2021, 2022a), we employed this model and found that GLORYS2V4 consistently delivers the most reliable outcomes when simulating the sub-thermocline circulation system across various regions in the western Pacific, notably around the MUC, EUC, NEUC, and STDCC regions, in comparison to other widely utilized reanalysis models like the Hybrid Coordinate Ocean Model (HYCOM) and the Oceanic General Circulation Model for the Earth Simulator (OFES). However, given the reliance on a single reanalysis product, caution is advised, especially in regions with limited observational data where the model might not accurately capture local oceanographic conditions.

EKE is a commonly used parameter to identify oceanic eddies by determining the kinetic energy of the time-varying component of the velocity. The EKE is simply computed as,

$$\mathrm{EKE} = \frac{u'^2 + v'^2}{2} \tag{1}$$

where (u' and v') are the zonal and meridional velocity anomalies relative to the time mean value from 1993 to 2020, respectively. However, this approach may capture a wide range of eddy variability, not solely isolating mesoscale signals. The second method is OWP, which is a classical approach for identifying eddies by assessing the relative contributions of deformation (i.e., shear strain and normal strain) and vorticity in the fluid flow. The OWP can be defined as follows,

$$\mathrm{OWP} = \left(\frac{\partial v}{\partial x} + \frac{\partial u}{\partial y}\right)^2 + \left(\frac{\partial u}{\partial x} - \frac{\partial v}{\partial y}\right)^2 - \left(\frac{\partial v}{\partial x} - \frac{\partial u}{\partial y}\right)^2 \tag{2}$$

where (u and v) are the zonal and meridional velocity, respectively, and (x and y) are the zonal and meridional coordinates, respectively.

In Equation 2, the first, second, and third parentheses on the right-hand side represent the shear strain, normal strain, and relative vorticity, respectively. The OWP method defines eddies when rotation predominates over deformation. Thus, a negative OWP value indicates the presence of an eddy. In the OWP method, the threshold value should be carefully specified by which eddies are defined depending on the eddy scale (Chelton et al., 2011). Setting the threshold too high (low) may remove small eddies (merge small eddies into one large eddy region). With a resolution of 0.25°, GLORYS2V4 partially resolves mesoscale eddies, particularly those with a length scale over 100 km (Hewitt et al., 2020), while completely neglecting submesoscale eddies. Hence, our study focuses solely on mesoscale SEs with a horizontal scale larger than 100 km and a lifetime exceeding 30 days. This is, of course, an incomplete representation of mesoscale SEs; however, it captures the dominant SEs in the western Pacific (Xu et al., 2019). Through several experiments, the threshold value of 4×10^{-13} was applied for the optimal identification of mesoscale SEs in the western Pacific (Figures S1a and S1b). To reduce the noise, a 1° × 1° spatial filter is applied horizontally. In this study, we only consider the negative OWP values to map the eddies based on their polarities. The positive OWP values, which correspond to non-eddy regions, are removed. The eddy polarities are then classified as follows,

$$\text{Cyclonic eddy}: \frac{\partial v}{\partial x} - \frac{\partial u}{\partial y} > 0 \tag{3}$$

$$\text{Anticyclonic eddy}: \frac{\partial v}{\partial x} - \frac{\partial u}{\partial y} < 0 \tag{4}$$

2.2. Baroclinic and Barotropic Energy Conversions

Adapted from Eden and Böning (2002), barotropic (BTC) and baroclinic (BCC) energy conversions can be calculated as follows,

$$\mathrm{BCC} = -\frac{g^2}{N^2\rho_0}\left(\overline{u'\rho'}\frac{\partial\overline{\rho}}{\partial x} + \overline{v'\rho'}\frac{\partial\overline{\rho}}{\partial y}\right) \tag{5}$$

$$\mathrm{BTC} = -\rho_0\left[\overline{u'^2}\frac{\partial\overline{u}}{\partial x} + \overline{v'^2}\frac{\partial\overline{v}}{\partial y} + \overline{u'v'}\left(\frac{\partial\overline{v}}{\partial x} + \frac{\partial\overline{u}}{\partial y}\right)\right] \tag{6}$$

where g, ρ, ρ_0, and $N^2\left(N \equiv \sqrt{-\frac{g}{\rho}\frac{\partial\rho}{\partial z}}\right)$ represent gravitational acceleration, density, background density (1,025 kg/m^3), and the square of the buoyancy frequency, respectively. The density was derived from the GLORYS2V4 model outputs of temperature and salinity. Variables with an upper bar and a prime symbol represent the time mean value over the full period of study (1993–2020) and the anomaly relative to the time mean value, respectively.

The BTC represents the energy conversion between the mean kinetic energy (MKE) and the EKE resulting from the horizontal shear instability of the background flow, whereas the BCC denotes the energy conversion between the eddy available potential energy (EAPE) and the mean available potential energy (MAPE) (Yan et al., 2019). A positive BTC (BCC) indicates that MKE (MAPE) is converted into EKE (EAPE), while a negative BTC and BCC signify the reverse direction of these respective energy transfers.

All calculations were conducted using depth coordinates. Subsequently, the depth coordinates of each derived parameter were regridded to isopycnal (σ_θ) coordinates using density values derived from temperature and salinity data sets obtained from GLORYS2V4.

3. Results and Discussion

Figure 2 presents the horizontal distributions of velocities, EKE, OWP, BCC, and BTC. The figure displays the mean state of each parameter using daily mean data from 1993 to 2020. To capture most SEs in the western Pacific, isopycnal layers ranging from 26.8 to 27.6σ_θ were chosen, as indicated by previous studies (Azminuddin et al., 2021; Qiu et al., 2013; Qu et al., 2012; Song et al., 2022; Xu et al., 2019). Consequently, at the equator, the Equatorial Undercurrent (EUC) is absent, and instead, the deeper eastward flows such as the South Subsurface Countercurrent (SSCC), the Equatorial Deep Jets (EDJs), and the North Subsurface Countercurrent (NSCC) emerge. Note that, not all eddies within this layer are necessarily SEs. Some of them may serve as vertical extensions of the surface eddies. Therefore, it is necessary to distinguish SEs from surface eddies. To exclude surface eddies, this study omitted eddies that exhibited intensification (minimum OWP) in the upper thermocline.

3.1. Western Pacific Basin

Below the thermocline, this region exhibits alternating zonal currents (Figure 2a). Previous studies have revealed a meridional pattern of eastward flows that shift northward with increasing depth, including the EUC, the NSCC, three cores of the NEUC, and the Subtropical Deep Countercurrent (STDCC) (Figure 2g) (Azminuddin et al., 2021; Y. Li et al., 2018; Nakano & Hasumi, 2005).

In the interior western Pacific basin, two regions exhibit relatively high EKE: the equatorial region and the latitudinal band between 9°N and 19°N, with a higher EKE existing closer to the western boundary (Figure 2c). Near the Philippine coast, the maximum EKE is centered at approximately 10.5°N, in agreement with Chiang et al. (2015). This core shifts northward further east, reaching around 14°N at 180°E. Although the high EKE is primarily concentrated in these two bands, the OWP results indicate the presence of SEs in nearly all regions (Figure 2d).

One interesting feature is that cyclonic and anticyclonic SEs have a meridional pattern that lines up with the latitudinal distribution of zonal undercurrents, including the SSCC, EDJ, NSCC, three cores of NEUC, and STDCC (Figures 2a, 2d, and 2h). This pattern is especially clear south of 25°N. This similar meridional pattern indicates a close association between the zonal undercurrents and the SEs.

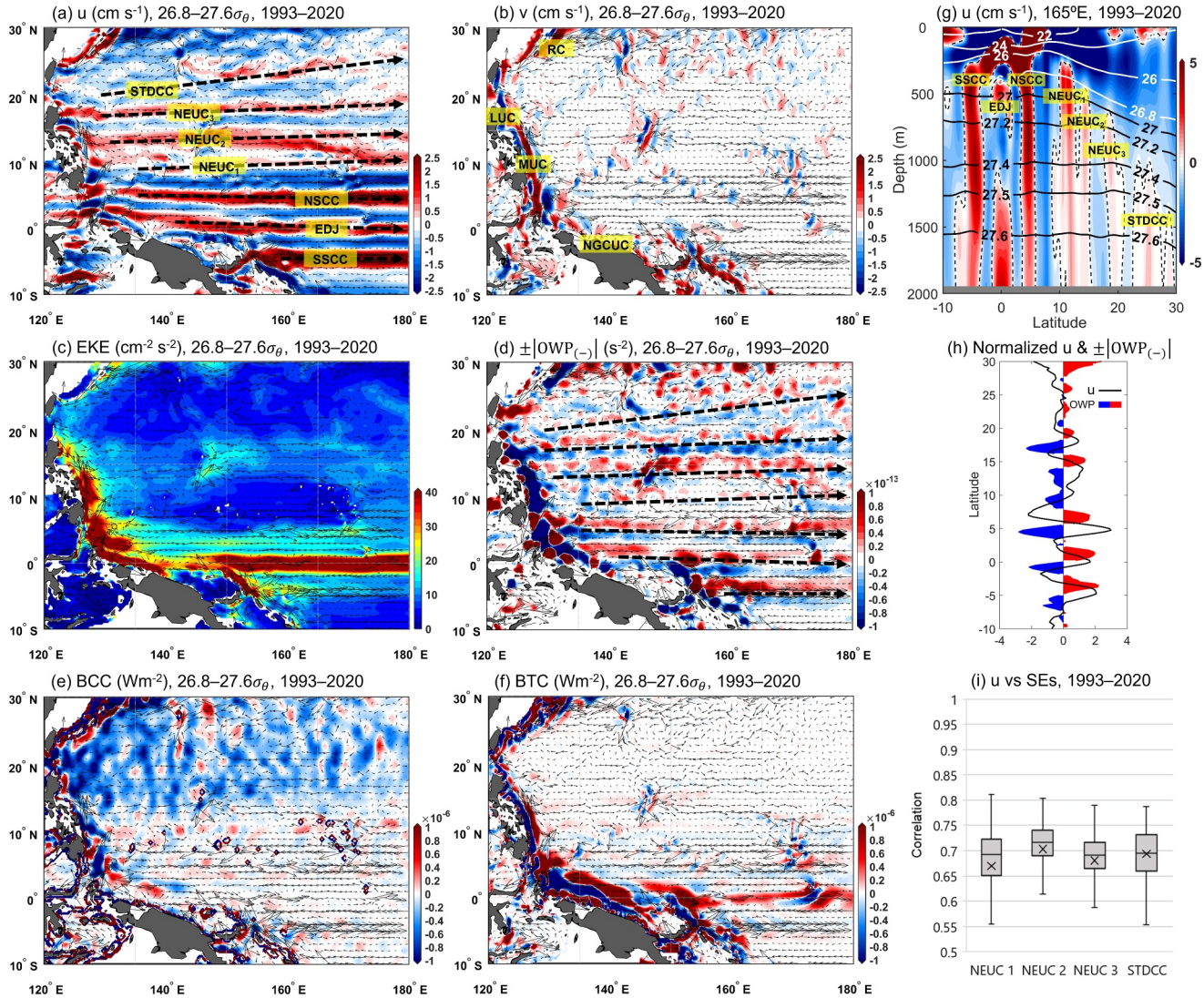

Figure 2. Horizontal distribution of (a) zonal velocity (cm s^{-1}), (b) meridional velocity (cm s^{-1}), (c) Eddy kinetic energy (cm^{-2} s^{-2}), (d) Okubo-Weiss parameter ($\pm|OWP_{(-)}|$, s^{-2}), (e) baroclinic energy conversion (W m^{-2}), and (f) barotropic energy conversion (W m^{-2}) averaged over 26.8–27.6σ_θ density layers and from 1993 to 2020. The black arrows represent current vectors. The dotted arrows in (a) and (d) indicate the location of selected subsurface eastward currents. (g) Latitude-depth section of zonal velocities (cm s^{-1}; color shading) and potential density (σ_θ; white and black contours) along 165°E from 1993 to 2020. Dashed contours in (g) denote the zero zonal velocity. (h) Latitude profile of the normalized zonal velocity (black line) and $\pm|OWP_{(-)}|$ (colored area) longitudinally using z-score normalization method averaged over the western Pacific interior basin. The red (blue) colors in (d) and (h) indicate the cyclonic (anticyclonic) eddy regions defined from $|OWP_{(-)}|$ with negative (positive) vorticity. (i) Box plot of correlation coefficients between zonal velocity and surrounding Subthermocline eddie events from 1993 to 2020 in the North Equatorial Undercurrent and Subtropical Deep Countercurrent regions. All parameters were estimated from GLORYS2V4.

Several possible mechanisms have been proposed to describe the dynamics of subsurface zonal flows in the western Pacific, including wind forcing, baroclinic instability, turbulence rectification, and baroclinic Rossby waves (Nakano & Hasumi, 2005; Nakano & Suginohara, 2002; Qiu et al., 2015). In this study, the similarity in the latitudinal distributions of zonal velocities and SEs presented in Figure 2 strongly supports the idea of an eddy-driven undercurrent mechanism, which is achieved through the convergence of eddy potential vorticity flux (Qiu et al., 2013; Rhines & Holland, 1979).

Notice that each eastward flow is situated between the cyclonic SEs to the north and anticyclonic SEs to the south. While the SEs propagate westward, most of them exhibit strong nonlinearity, with their average rotational speed surpassing their translation speed (Xu et al., 2019). As a result, the time-mean zonally elongated eastward velocity

may arise from the convergence of cyclonic swirling motions from the north and anticyclonic swirling motions from the south.

The reason behind the meridional pattern of cyclonic and anticyclonic SEs remains unclear and needs further investigation. It is possible that the northern (southern) side of the eastward flow preferentially sheds vortices with cyclonic (anticyclonic) rotation. This is particularly plausible for the undercurrents around the equator, considering their relatively strong flow (Figure 2g). However, the NEUC and STDCC are too weak to generate SEs (Qiu et al., 2013). Figure 2d shows a discontinuous meridional pattern of SEs, particularly between 5°N and 12°N to the west of 170°E. The topographic features around 160°E–170°E, 5°N–12°N (Marshall Islands) appear to obstruct the westward propagating SEs, as indicated by the low EKE and OWP to the west of this topographic formation (Figures 2c and 2d). This obstruction may account for the observed weakness in the southern core of the NEUC ($NEUC_1$, ~10°N) to the west of 170°E. In addition, the zonal undercurrents, which are observed more as laminar flows with a zonally elongated pattern in the time-mean state (Figure 2a), act a little bit randomly at times, likely attributed to the presence of numerous eddies (Figure S1). This implies that the position of these zonal jets is not stable over time. Therefore, in this region, eddies are not likely sourced from the mean flow. Instead, the westward propagating SEs significantly influence the formation of the mean zonal flows. Wind-driven Rossby waves likely influence the propagation pattern of SEs and help establish the structure of the off-equatorial zonal jets through the convergence of eddy potential vorticity flux.

In terms of temporal changes, we assessed whether changes in zonal current strength relate to nearby SE activity by comparing the time series of zonal velocity and EKE of certain SEs along the STDCC and NEUC cores with a mean velocity greater than 0.5 cm s^{-1}. In this analysis, we only consider SEs within 100 km from the respective eastward velocity core. Positive (negative) correlations were defined when the time series of EKE north (south) of the eastward cores lined up with changes in zonal currents, with cyclonic (anticyclonic) SEs identified as positive (negative) EKE. The results show a robust connection between zonal velocity and nearby SE activities in the NEUC and STDCC regions, with an average correlation coefficient of approximately 0.7 (Figure 2i). This confirms that intensified eastward velocity coincides with cyclonic (anticyclonic) SE to the north (south), while weaker eastward flows correspond to the opposite trend, suggesting that SE recirculation has a significant effect on how these undercurrents change over time.

To further examine the interaction between SEs and mean flow, we conducted analyses of BTC and BCC energy conversions (see Figures 2e and 2f). In the interior basin, positive BTC and negative BCC predominantly characterize the equatorial and off-equatorial regions, respectively. Conversely, the BTC (BCC) weakens in higher (lower) latitude regions. This result indicates that the dynamics of the zonal undercurrent system in the equatorial region differ from those in the tropical-subtropical region.

The eddy-driven mean flow, facilitated by the convergence of eddy potential vorticity flux mechanism through baroclinic energy conversion, is specifically applicable to the eastward-flowing NEUC and STDCC, as evidenced by the negative BCC. In contrast, the equatorial zonal flows appear to induce the formation of SEs primarily through horizontal shear instability, leading to barotropic energy conversion, as indicated by a strong positive BTC along the equator. This is reasonable, considering that the undercurrents around the equator are much stronger than those at higher latitudes (Figure 2g). However, the forcings that set up these currents, which remains one of the great challenges in physical oceanography, falls outside the scope of this study. The different ways that zonal undercurrents work in the equatorial region compared to the tropical-subtropical region are consistent with the findings of Menesguen et al. (2019).

3.2. Western Boundary Region

The Pacific western boundary region features intricate surface and subsurface circulation systems. Those include the Kuroshio Current (KC), the Mindanao Current, and the New Guinea Coastal Current at the upper layer, and the Ryukyu Current (RC), the Luzon Undercurrent (LUC), the Mindanao Undercurrent (MUC), and the New Guinea Coastal Undercurrent (NGCUC) below the surface (Figure 1). These boundary currents, which are directly exposed to the open ocean, are highly susceptible to the influence of propagating eddies, primarily originating from the east (e.g., Chiang et al., 2015; Xu et al., 2019).

Figure 2c shows a high EKE along the western boundary, indicating a high concentration of SEs. Among all regions, the Philippine coast exhibits the most intense SE activities. Chiang et al. (2015) suggested two groups of

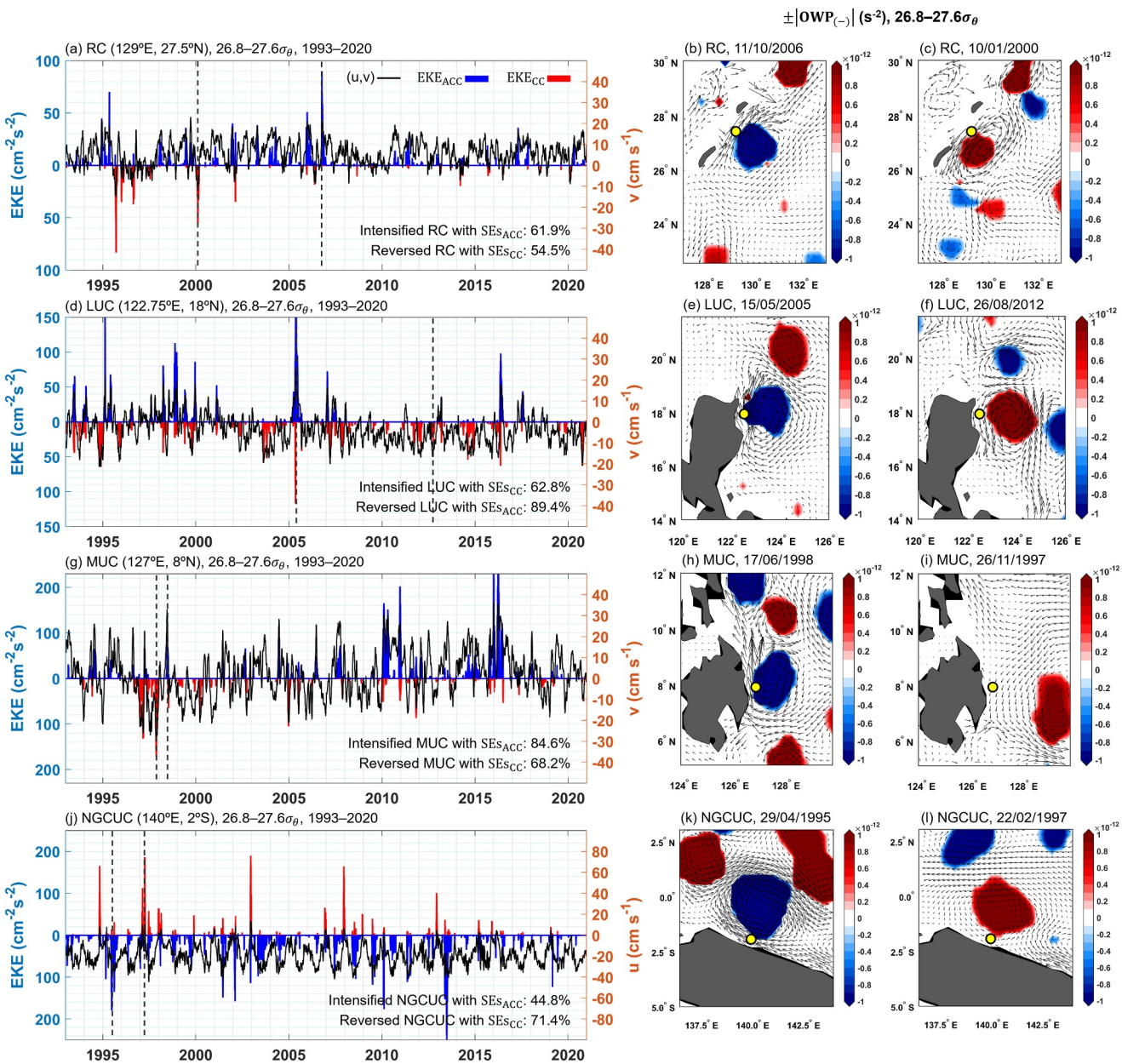

Figure 3. Time series of velocity (cm s^{-1}) (black line) of (a) the Ryukyu Current, (d) the Luzon Undercurrent, (g) the Mindanao Undercurrent, and (j) the New Guinea Coastal Undercurrent from 1993 to 2020. The velocity values were estimated at the location indicated by the yellow circle in the corresponding right panels. The red and blue colors represent the time series of cyclonic and anticyclonic eddy kinetic energy (cm^{-2} s^{-2}), respectively, averaged over 26.8–27.6σ_θ density layers and spanning two degrees offshore from the yellow circle. The second- and third-column panels display snapshots of Okubo-Weiss parameter ($\pm|OWP_{(-)}|$, s^{-2}) averaged over 26.8–27.6σ_θ density layers on (b) 11 October 2006, (c) 10 February 2000, (e) 15 May 2005, (f) 26 August 2012, (h) 17 June 1998, (i) 26 October 1993, (k) 29 June 1995, and (l) 22 October 1997. The black arrows represent current vectors. The vertical dashed lines in the first-column panels indicate the timing of snapshots in the second- and third-column panels.

SEs near the Philippine coast: one originating from the central Pacific and the other from the New Guinea coast. Previous studies also noted a distinct anticyclonic SE southeast of Mindanao Island (Azminuddin, Lee, et al., 2022; L. Zhang et al., 2021). While its presence remains uncertain, the establishment of this eddy is potentially due to the tilting of the Halmahera Eddy poleward with increasing depth (Kashino et al., 2013).

Early hydrographic observations have provided evidence for the significant contribution of SEs to the variations of Pacific western boundary undercurrents (Ma et al., 2022; Yan et al., 2019; L. Zhang et al., 2014). To assess SE-undercurrent interactions, we analyze the time series of velocity and EKE for each undercurrent (Figures 3a, 3d,

3g, and 3j). The results show that anticyclonic SEs typically coincide with intensified northward-flowing boundary currents (i.e., RC, MUC, NGCUC), while cyclonic SEs are associated with intensified southward-flowing boundary currents (i.e., LUC). The findings also confirm that SE with opposite polarity typically exists during the reversed flow of these undercurrents. For example, during a strong southward-flowing LUC event on 28 August 2012, the model results confirm that the subthermocline southward current east of Luzon Island was part of the recirculation associated with a cyclonic SE, as shown in Figure 3f. In contrast, an anticyclonic SE can temporarily reverse the water flow, causing it to become northward in this region (Figure 3e).

Energy conversion analysis results (Figures 2e and 2f) confirm that along the western boundary, SEs contribute to energy transfer to the mean flow primarily through barotropic instability, as indicated by negative BTC, particularly east of the Ryukyu Islands and the Philippine coast, in agreement with Yan et al. (2019). Abundant anticyclonic SEs east of the Ryukyu Islands (Figures 2d and 3c) supply energy to the background mean flow, enhancing the northward-flowing RC, in which the inverse energy cascade provides a route for SEs to dissipate during their interactions with the RC. In contrast, the presence of cyclonic SEs would reverse this current.

The pronounced negative values of both BTC and BCC along the Philippine coast confirm the conversion of kinetic and potential energies from SEs into the mean flow through barotropic and baroclinic instabilities, respectively. This affirms that the prevailing anticyclonic SEs along the Philippine coast (Figure 2d) provide energy to the background mean flow, strengthening the northward-flowing MUC and potentially contributing to its generation (Qiu et al., 2015). These incoming SEs are intensified by background shear instability near the Philippine coast, leading to high EKE, potentially causing intermittent northward-flowing MUC (Figure 3g). In the same way, cyclonic (anticyclonic) SEs intensify (reverse) the southward-flowing LUC east of Luzon Island (Figure 3d).

Not all SEs along the western boundary originate from the east; some are locally generated, as indicated by positive BTC following negative BTC east of the Ryukyu Islands and the Philippine coast, signifying the conversion of MKE to EKE due to horizontal shear instability of the background flow near the coast. Conversely, along the New Guinea coast, positive BTC exists near the coast followed by negative BTC, indicating that, near the coast, energy is primarily transferred from the MKE to EKE through the shear stress exerted by the existing undercurrent (i.e., NGCUC). In this region, SEs often form due to the interaction of ocean currents with the complex bathymetry and topography of the area (Chiang & Qu, 2013). The presence of the Ninigo Group (a group of atolls, islands, and reefs) creates favorable conditions for SE generation primarily through barotropic instability. Negative BTC in the area away from the coast indicates that the SEs could have a feedback influence on MKE along the New Guinea coast, potentially affecting NGCUC pathways and undercurrent linkages (Azminuddin, Jang, & Jeon, 2022).

To quantify the contribution of SEs to the modulation of boundary undercurrents, we compare the time series of current velocity and SE events. Subsequently, we calculate the percentage of strong and weak (reversed) events in each undercurrent that are associated with SE recirculation (Figures 3a, 3d, 3g, & 3j). We select a velocity of 10 cm/s (MUC, LUC, and RC) and 20 cm/s (NGCUC) to denote strong events. Weak events are identified when the velocity reverses.

The results show that SEs significantly influence the variations in most western boundary undercurrents. This is especially true for the MUC, the LUC, and the RC, where SEs are responsible for over 54% of their strengthening and weakening. Notably, anticyclonic SEs contribute to 84.6% (89.4%) of the MUC (LUC) intensification (reversal), emphasizing their crucial role in the variation of undercurrents east of the Philippine coast. These findings, along with the results of the energy conversion analysis, strongly support the idea that SEs exert a pronounced influence on these currents. Specifically, anticyclonic SEs typically enhance (reverse) the velocity of boundary undercurrents flowing northward (southward), while cyclonic SEs do the opposite.

Figure 1 displays a schematic map illustrating the circulation system in the western Pacific. Note that, in Figure 1, we exclude surface eddies, with the exception of two quasi-stationary eddies, that is, the Halmahera and Mindanao eddies. By this map, we emphasize that while individual undercurrent systems in the western Pacific possess their unique properties, it is beneficial to consider them in an interconnected framework, particularly through mutual interactions and external forcing. An external force that is fundamental to the dynamics of these undercurrents is SEs. We believe that this point of view is essential to advance scientific knowledge of the underlying processes below the surface in the Pacific and global oceans.

4. Conclusions

SEs are widespread in the western Pacific, with notable concentrations east of the Philippine coast, east of the Ryukyu Islands, the equatorial region, and within the latitudinal band between 9°N and 19°N. While SEs are increasingly recognized for their influence on ocean circulation, their significant impact on the regional undercurrent system in the western Pacific remains largely unexplored and, in some regions, often underestimated. Using reanalysis model outputs, this study emphasizes the extensive impacts of SEs in regulating the formation and variation of undercurrent systems in the western Pacific.

A meridional pattern of cyclonic and anticyclonic SEs distribution in the interior western Pacific aligns with zonally elongated undercurrents, indicating their close association. The OWP and energy conversion results indicate that nonlinear mesoscale SEs play a role in regulating the formation of tropical-subtropical undercurrents, particularly the NEUC and the STDCC, primarily through baroclinic energy conversion and the convergence of eddy potential vorticity flux. The time-mean eastward flow arises from the convergence of cyclonic (anticyclonic) swirling motions from the north (south).

Along the western boundary, undercurrents east of the Ryukyu Islands and the Philippine coast, directly exposed to the open ocean, are highly influenced by incoming SEs primarily from the east. The SEs impinge on the western boundary, leading to significant variation in the intensity and structure of the undercurrent system, particularly the RC, the LUC, and the MUC, where over 54% of their intensification and reversal are attributed to SEs. Our findings confirm that anticyclonic SEs typically enhance (reverse) the velocity of boundary currents flowing northward (southward) primarily through barotropic energy conversion, while cyclonic SEs do the opposite.

Data Availability Statement

The data on which this article is based are available at GLORYS2V4 (2023).

Acknowledgments

This research was supported by Korea Institute of Marine Science & Technology (KIMST) funded by the Ministry of Oceans and Fisheries ("KIOS (Korea Indian Ocean Study): Korea-US Joint Observation Study of the Indian Ocean (20220548, PM63990)," "Development of risk managing technology tackling ocean and fisheries crisis around Korean Peninsula by Kuroshio Current (RS-2023-00256330)," and "Korea-China Joint Ocean Research Center (20220407)"). This work is also supported by the Physical Oceanography program of U.S. National Aeronautics and Space Administration (NASA; Grant 80NSSC18K0777) and National Science Foundation (NSF; Grant 2242151) through the University of Maryland for R.D.S.

References

Azminuddin, F., Jang, C. J., & Jeon, D. (2022). Destination of New Guinea coastal undercurrent in the Western tropical Pacific: Variability and linkages. *Frontiers in Marine Science*, *9*, 1080314. https://doi.org/10.3389/fmars.2022.1080314

Azminuddin, F., Jeon, D., Kim, Y. H., Jang, C. J., & Park, J.-H. (2021). A newly observed deep countercurrent in the subtropical northwest Pacific. *Journal of Geophysical Research: Oceans*, *126*(7), e2021JC017272. https://doi.org/10.1029/2021JC017272

Azminuddin, F., Lee, J. H., Jeon, D., Shin, C.-W., Villanoy, C., Lee, S., et al. (2022). Effect of the intensified sub-thermocline eddy on strengthening the Mindanao Undercurrent in 2019. *Journal of Geophysical Research: Oceans*, *127*(2), e2021JC017883. https://doi.org/10.1029/2021JC017883

Beech, N., Rackow, T., Semmier, T., Danilov, S., Wang, Q., & Jung, T. (2022). Long-term evolution of ocean eddy activity in a warming world. *Nature Climate Change*, *12*, 910–917. https://doi.org/10.1038/s41558-022-01478-3

Chelton, D. B., Schlax, M. G., & Samelson, R. M. (2011). Global observations of nonlinear mesoscale eddies. *Progress in Oceanography*, *91*(2), 167–216. https://doi.org/10.1016/j.pocean.2011.01.002

Chiang, T.-L., & Qu, T. (2013). Subthermocline eddies in the Western equatorial Pacific as shown by an eddy-resolving OGCM. *Journal of Physical Oceanography*, *43*(7), 1241–1253. https://doi.org/10.1175/JPO-D-12-0187.1

Chiang, T.-L., Wu, C.-R., Qu, T., & Hsin, Y.-C. (2015). Activities of 50–80 day subthermocline eddies near the Philippine coast. *Journal of Geophysical Research: Oceans*, *120*(5), 3606–3623. https://doi.org/10.1002/2013JC009626

Cravatte, S., Kessler, W. S., & Marin, F. (2012). Intermediate zonal jets in the tropical Pacific ocean observed by Argo floats. *Journal of Physical Oceanography*, *42*(9), 1475–1485. https://doi.org/10.1175/JPO-D-11-0206.1

Danabasoglu, G., McWilliams, J. C., & Gent, P. R. (1994). The role of mesoscale tracer transports in the global ocean circulation. *Science*, *264*(5162), 1123–1126. https://doi.org/10.1126/science.264.5162.1123

Delpech, A., Cravatte, S., Marin, F., Morel, Y., Gronchi, E., & Kestenare, E. (2020). Observed tracer fields structuration by middepth zonal jets in the tropical Pacific. *Journal of Physical Oceanography*, *50*(2), 281–304. https://doi.org/10.1175/JPO-D-19-0132.1

Eden, C., & Böning, C. (2002). Sources of eddy kinetic energy in the Labrador sea. *Journal of Physical Oceanography*, *32*(12), 3346–3363. https://doi.org/10.1175/1520-0485(2002)032<3346:SOEKEI>2.0.CO;2

GLORYS2V4. (2023). Global Ocean Ensemble Physics reanalysis. E.U. Copernicus marine Service information (CMEMS) [Dataset]. *Marine Data Store (MDS)*. https://doi.org/10.48670/moi-00024

Hewitt, H. T., Roberts, M., Mathiot, P., Biastoch, A., Blockley, E., Chassignet, E. P., et al. (2020). Resolving and parameterising the ocean mesoscale in Earth system models. *Current Climate Change Reports*, *6*(4), 137–152. https://doi.org/10.1007/s40641-020-00164-w

Hu, D., & Cui, M. (1991). The Western boundary current of the Pacific and its role in the climate. *Chinese Journal of Oceanology and Limnology*, *9*(1), 1–14. https://doi.org/10.1007/BF02849784

Hu, D., Wang, F., Sprintall, J., Wu, L., Riser, S., Cravatte, S., et al. (2020). Review on observational studies of Western tropical Pacific Ocean circulation and climate. *Journal of Oceanology and Limnology*, *38*(4), 906–929. https://doi.org/10.1007/s00343-020-0240-1

Kashino, Y., Atmadipoera, A., Kuroda, Y., & Lukijanto. (2013). Observed features of the Halmahera and Mindanao eddies. *Journal of Geophysical Research: Oceans*, *118*(12), 6543–6560. https://doi.org/10.1002/2013JC009207

Li, X., Yang, Y., Li, R., Zhang, L., & Yuan, D. (2020). Structure and dynamics of the Pacific North Equatorial subsurface current. *Scientific Reports*, *10*(1), 11758. https://doi.org/10.1038/s41598-020-68605-y

Li, Y., Liu, H., & Lin, P. (2018). Interannual and decadal variability of the North Equatorial Undercurrents in an eddy-resolving ocean model. *Scientific Reports*, *8*(1), 17112. https://doi.org/10.1038/s41598-018-35469-2

Ma, J., Hu, S., Hu, D., Villanoy, C., Wang, Q., Lu, X., & Yuan, X. (2022). Structure and variability of the Kuroshio and Luzon undercurrent observed by a mooring Array. *Journal of Geophysical Research: Oceans*, *127*(2), e2021JC017754. https://doi.org/10.1029/2021JC017754

McCoy, D., Bianchi, D., & Stewart, A. L. (2020). Global observations of submesoscale coherent vortices in the ocean. *Progress in Oceanography*, *189*, 102452. https://doi.org/10.1016/j.pocean.2020.102452

McWilliams, J. C. (2008). The nature and consequences of oceanic eddies. *Geophysical Monograph Series*, *177*, 5–15. https://doi.org/10.1029/177gm03

Menesguen, C., Delpech, A., Marin, F., Cravatte, S., Schopp, R., & Morel, Y. (2019). Observations and mechanisms for the formation of deep equatorial and tropical circulation. *Earth and Space Science*, *6*(3), 370–386. https://doi.org/10.1029/2018EA000438

Nakano, H., & Hasumi, H. (2005). A Series of zonal jets embedded in the broad zonal flows in the Pacific obtained in eddy-permitting ocean general circulation models. *Journal of Physical Oceanography*, *35*(4), 474–488. https://doi.org/10.1175/JPO2698.1

Nakano, H., & Suginohara, N. (2002). A series of Middepth zonal flows in the Pacific driven by winds. *Journal of Physical Oceanography*, *32*(1), 161–176. https://doi.org/10.1175/1520-0485(2002)032<0161:ASOMZF>2.0.CO;2

Nan, F., Yu, F., Wei, C. J., Ren, Q., & Fan, C. H. (2017). Observations of an extra-large subsurface anticyclonic eddy in the northwestern Pacific subtropical gyre. *Journal of Marine Science: Research & Development*, *7*(04), 234. https://doi.org/10.4172/2155-9910.1000234

Qiu, B., Chen, S., Rudnick, D. L., & Kashino, Y. (2015). A New Paradigm for the North Pacific subthermocline low-latitude Western boundary current system. *Journal of Physical Oceanography*, *45*(9), 2407–2423. https://doi.org/10.1175/JPO-D-15-0035.1

Qiu, B., Chen, S., & Sasaki, H. (2013). Generation of the North equatorial undercurrent jets by triad baroclinic Rossby wave interactions. *Journal of Physical Oceanography*, *43*(12), 2682–2698. https://doi.org/10.1175/JPO-D-13-099.1

Qu, T., Chiang, T.-L., Wu, C.-R., Dutrieux, P., & Hu, D. (2012). Mindanao current/undercurrent in an eddy-resolving GCM. *Journal of Geophysical Research*, *117*(C6), C06026. https://doi.org/10.1029/2011JC007838

Raeisi, A., Bidokhti, A., Nazemosadat, S. M. J., & Lari, K. (2020). Mesoscale eddies and their dispersive environmental impacts in the Persian Gulf. *Chinese Physics B*, *29*(8), 084701. https://doi.org/10.1088/1674-1056/ab96a3

Rhines, P. B., & Holland, W. R. (1979). A theoretical discussion of eddy-driven mean flows. *Dynamics of Atmospheres and Oceans*, *3*(2–4), 289–325. https://doi.org/10.1016/0377-0265(79)90015-0

Richardson, P. L., Bower, A. S., & Zenk, W. (2000). A census of Meddies tracked by floats. *Progress in Oceanography*, *45*(2), 209–250. https://doi.org/10.1016/s0079-6611(99)00053-1

Robinson, A. R. (1983). *Eddies in marine science* (p. 609). Springer-Verlag. https://doi.org/10.1007/978-3-642-69003-7

Song, W., Zhang, L., & Hu, D. (2022). Observed subsurface lens-like features east of the Philippines. *Deep-Sea Research I*, *190*, 103901. https://doi.org/10.1016/j.dsr.2022.103901

Thomsen, S., Kanzow, T., Krahmann, G., Greatbatch, R. J., Dengler, M., & Gaute, L. (2016). The formation of a subsurface anticyclonic eddy in the Peru-Chile Undercurrent and its impact on the near-coastal salinity, oxygen, and nutrient distributions. *Journal of Geophysical Research: Oceans*, *121*(1), 476–501. https://doi.org/10.1002/2015JC010878

Thoppil, P. G., Metzger, E. J., Hurlburt, H. E., Smedstad, O. M., & Ichikawa, H. (2016). The current system of the Ryukyu Islands as revealed by a global ocean reanalysis. *Progress in Oceanography*, *141*, 239–258. https://doi.org/10.1016/j.pocean.2015.12.013

Wang, F., Song, L., Li, Y., Liu, C., Wang, J., Lin, P., et al. (2016). Semiannually alternating exchange of intermediate waters east of the Philippines. *Geophysical Research Letters*, *43*(13), 7059–7065. https://doi.org/10.1002/2016GL069323

Wang, Q., Pang, C., & Dong, C. (2022). Role of submesoscale processes in the isopycnal mixing associated with subthermocline eddies in the Philippine Sea. *Deep Sea Research Part II*, *202*, 105148. https://doi.org/10.1016/j.dsr2.2022.105148

Xu, A., Yu, F., & Nan, F. (2019). Study of subsurface eddy properties in northwestern Pacific Ocean based on an eddy-resolving OGCM. *Ocean Dynamics*, *69*(4), 463–474. https://doi.org/10.1007/s10236-019-01255-5

Yan, X., Kang, D., Curchitser, E. N., & Pang, C. (2019). Energetics of eddy-mean flow interactions along the Western boundary currents in the North Pacific. *Journal of Physical Oceanography*, *49*(3), 789–810. https://doi.org/10.1175/JPO-D-18-0201.1

Yang, Y., Wang, D., Wang, Q., Zeng, L., Xing, T., He, Y., et al. (2019). Eddy-induced transport of saline Kuroshio water into the northern south China sea. *Journal of Geophysical Research: Oceans*, *124*(9), 6673–6687. https://doi.org/10.1029/2018JC014847

Zhang, L., Hu, D., Hu, S., Wang, F., Wang, F., & Yuan, D. (2014). Mindanao Current/Undercurrent measured by a subsurface mooring. *Journal of Geophysical Research: Oceans*, *119*(6), 3617–3628. https://doi.org/10.1002/2013JC009693

Zhang, L., Hui, Y., Qu, T., & Hu, D. (2021). Seasonal variability of subthermocline eddy kinetic energy east of the Philippines. *Journal of Physical Oceanography*, *51*(3), 685–699. https://doi.org/10.1175/JPO-D-20-0101.1

Zhang, Z., Zhang, Y., & Wang, W. (2017). Three-compartment structure of subsurface-intensified mesoscale eddies in the ocean. *Journal of Geophysical Research: Oceans*, *122*(3), 1653–1664. https://doi.org/10.1002/2016JC012376